Vet Pathol **40**:659–669 (2003)

Glioblastoma Multiforme: Clinical Findings, Magnetic Resonance Imaging, and Pathology in Five Dogs

D. LIPSITZ, R. J. HIGGINS, G. D. KORTZ, P. J. DICKINSON, A. W. BOLLEN, D. K. NAYDAN, AND R. A. LECOUTEUR

Departments of Surgical and Radiological Sciences (DL, GDK, PJD, RAL) and Pathology, Microbiology, and Immunology (RJH) and Veterinary Medical Teaching Hospital (DKN), School of Veterinary Medicine, University of California–Davis, Davis, CA; and
Department of Pathology, School of Medicine, University of California–San Francisco, San Francisco, CA (AWB)

Abstract. Although glioblastoma multiforme (GBM), a World Health Organization grade IV astrocytoma, is the most common primary brain tumor in humans, in dogs GBM is relatively rare, accounting for only about 5% of all astrocytomas. This study presents combined clinical, neuroimaging, and neuropathologic findings in five dogs with GBM. The five dogs, aged from 5 to 12 years, were presented with progressive neurologic deficits that subsequent clinical neurologic examination and neuroimaging studies by magnetic resonance imaging (MRI), localized to space occupying lesions in the brain. MRI features of the tumors included consistent peritumoral edema ($n = 5$), sharp borders ($n = 4$), ring enhancement ($n = 3$), heterogenous T2-weighted signal intensity ($n = 3$), iso- to hypointense T1-weighted images ($n = 5$), necrosis ($n = 5$), and cyst formation ($n = 2$). Two tumors were diagnosed clinically using a computed tomography–guided stereotactic biopsy procedure. At necropsy all the tumors resulted in, on transverse sections, a prominent midline shift and had a variegated appearance due to intratumoral necrosis and hemorrhage. Histologically, they had serpentine necrosis with glial cell pseudopalisading and microvascular proliferation, features which distinguish human GBM from grade III astrocytomas. Immunoreactivity of tumor cells for glial fibrillary acidic protein was strongly positive in all cases, whereas 60% and 40% of the tumors also expressed epidermal growth factor receptor and vascular endothelial growth factor, respectively. These canine GBMs shared many diagnostic neuroimaging, gross, microcopic, and immunoreactivity features similar to those of human GBMs.

Key words: Astrocytoma; brain tumor; EGFR; glioblastoma multiforme; immunocytochemistry; magnetic resonance imaging; VEGF.

Glioblastoma multiforme (GBM), a World Health Organization (WHO) grade IV astrocytoma, is the most common human brain tumor comprising about 12–15% of all primary central nervous system (CNS) tumors and accounting for about 50–60% of all astrocytomas.[4,12,13] For diagnostic neuroimaging of human GBM, magnetic resonance imaging (MRI) is considered more useful than computed tomography (CT).[2,21] The basic MRI features of signal heterogeneity, necrosis, and hemorrhage are considered at least diagnostically suggestive of GBM.[2,21] The histologic and immunocytochemical criteria for their neuropathologic diagnosis from CT-guided stereotactic and surgical biopsy tissue and from necropsy examination are clearly defined.[4,12] In contrast, in dogs, astrocytomas form about 10% of all CNS tumors, and GBM represents only about 5% of all astrocytomas.[15,28] There are few reports of canine GBM, none of which describe combined clinical, MRI, and neuropathologic findings.[17,18,26] Also, because the expression of vascular endothelial growth factor (VEGF) and epidermal growth factor receptor (EGFR) is deregulated in many human GBMs representing potential therapeutic targets, we have studied their expression in the canine tumors.[3,7,12,19,20] This study of five spontaneous canine GBMs demonstrated close similarities between the MRI and neuropathologic findings in these dogs and those of human GBMs.

Materials and Methods

Clinical examination

Five dogs with a history of progressive neurologic disease were examined either at the University of California–Davis Veterinary Medical Teaching Hospital (dog nos. 1, 2, 4, and 5) or at the Emergency Animal Hospital and Referral Center in San Diego, CA (dog no. 3).

Each dog had a complete blood count, serum chemistry profile, urinalysis, thoracic radiographs, and abdominal ultrasound done. MRI of the head was done once on each dog using a 0.4-T scanner (Resonex 5000, Resonex Inc., Sunnyvale, CA) except for dog no. 5, which was imaged six times over a 3-month period as part of a clinical study. The imaging sequences were obtained from transverse 5-mm

slices with an interslice gap of 1 mm generated with T1-weighted (T1W); T2-weighted (T2W), and proton density–weighted (PDW) spin-echo pulse sequences. T1W images were also acquired after the intravenous administration of gadolinium-diethylenetriaminepenta-acetic acid (Gd-DTPA) (Magnevist, Berlex Laboratories, Wayne, NJ) at 0.2 mmol/kg, as described previously.[1] Cerebrospinal fluid (CSF) was obtained from the cerebellomedullary cistern immediately after MRI for routine analysis in dog nos. 1, 2, and 5. Dog nos. 1 and 5 also had CT-guided stereotactic brain biopsies done at 4 and 14 days after their MRI studies, respectively, as described previously.[10,14,30]

Pathology and immunocytochemistry

All dogs had a complete necropsy examination. Subsequently, tissues were immersed in 10% buffered formal saline before routine embedding in paraffin and subsequent microscopic evaluation of 5-μm-thick hematoxylin and eosin–stained sections. Smears and histologic tissues from the stereotactic biopsy samples were prepared and stained as described previously.[30]

Immunocytochemical staining was done on sections from selected tissues of each case with antibodies to glial fibrillary acidic protein (GFAP), human von Willebrand factor VIII, MIB-1, α-smooth muscle actin (SMA), vimentin, and pan cytokeratins (Lu-5), as reported previously.[6] The proliferative index from MIB-1 immunostaining was expressed in percent and derived by counting the number of positively stained nuclei in 1,000 tumor cells pooled from 5 to 10 fields (each 0.16 mm^2) examined at high-power magnification. The fields were selected from areas that had the highest density of positively reactive nuclei. In addition, using the same immunocytochemical procedure, with appropriate positive and negative controls, we applied the following antibodies: mouse monoclonal antibody (Mab) to human endothelial cell CD31 from Dako Corp. (Carpinteria, CA; clone JC/70A) at 1 : 50; mouse Mab to human VEGF from BD Biosciences (San Diego, CA; clone G153-694) at 1 : 200; and mouse Mab to human EGFR Calbiochem Corp. (San Diego, CA; clone 158) at 1 : 200. Terminal deoxynucleotidyl transferase–mediated deoxyuridine triphosphate nick end–labeling histochemical assay using the ApopTag detection kit (Intergen Co., Purchase, NY) was done according to the manufacturer's instructions. Tissue sections used in parallel as positive controls for immunoreactivity for VEGF and EGFR were obtained from a case of human GBM demonstrated to be immunoreactive to the same antibodies applied in another laboratory (Bollen, personal observation).

Results

Clinical findings

The five dogs presented with clinical signs referable to a focal lesion either in the thalamus or the cerebrum (dog nos. 1, 3, 4, and 5) or in the cerebellum/brainstem (dog no. 2). The essential data from signalment, historical, and neurologic examination are summarized in Table 1.

Complete blood counts, serum chemistries, urinalyses, thoracic radiographs and abdominal ultrasound examinations were unremarkable except in dog no. 2. This dog had a mature neutrophilia with a degenerative left shift and slight toxicity. On thoracic radiographs, the cervical and thoracic esophagus was dilated, and this finding was confirmed at necropsy.

Magnetic resonance imaging

Dog no. 1. Transverse MR images of the brain corresponded to the same slice level as that of the gross necropsy examination (Fig. 1a). On transverse T2W images, there was a large, hyperintense lesion extending from the pituitary fossa dorsally and bilaterally into the middle of the hypothalamus and thalamus (Fig. 1b). The lesion extended to the ventral surface of the lateral ventricles and obliterated the third ventricle. On transverse T1W images, the lesion was iso- to hypointense (Fig. 1c). There were also two hypointense areas corresponding to a cyst, and an area of necrosis was found at necropsy. (Fig. 1a, c). The lesion had marked uniform contrast enhancement that was smaller than the area of hyperintensity on T2W images (Fig. 1d).

Dog no. 2. On the transverse T2W and PDW images, there was a large mostly hyperintense lesion involving mainly the right pons and medulla, extending into the cerebellum on the right side. On the transverse T1W images, the lesion was iso- to hypointense and displaced the fourth ventricle dorsally to the left. The lesion had a thick ring of contrast enhancement in the brainstem and the cerebellum (Fig. 2), but the area of enhancement was smaller than the hyperintensity noted on the T2W and PDW images.

Dog no. 3. On transverse T2W and PDW images, there was a large hyperintense lesion in the white matter of the right frontal and parietal lobes, compressing the right lateral ventricle at the level of the caudate nucleus. There was a mass effect distorting the left lateral ventricle. On transverse T1W images, the lesion was iso- to hypointense. The lesion had a thin rim of contrast enhancement (Fig. 3).

Dog no. 4. On transverse T2W and PDW images, there was a large hyperintense lesion in the right olfactory bulb and right frontal lobe extending caudally into the thalamus and the lateral ventricle at the level of the interventricular foramen. The hyperintensity also extended into the deep medial portion of the left frontal lobe. On transverse T1W images, the lesion was hypointense, and there was moderate ventriculomegaly of the lateral, third and fourth ventricles. The lesion had a thick ring of contrast enhancement (Fig. 4).

Dog no. 5. This dog was imaged six times during a 3-month period as part of a separate study protocol. On transverse T2W and PDW images there was a large hyperintense lesion in the right frontal lobe, with sig-

Table 1. Signalment, history, and neurologic findings in five dogs with GBM.

Dog No.	Signalment	History	Neurologic Examination	Neuroanatomic Localization
1	Nine-year-old female spayed mixed breed	Two-month history of seizures, inappetence, and behavioral changes	Abnormal posture with head held low	Cerebral or thalamic
2	Five-year-old female spayed German Shepherd	Two-week history of excessive drooling, regurgitation, generalized ataxia, and right head tilt	Obtunded, generalized ataxia, right hemiparesis and leaning to right. Absent menace response oculus dexter (OD) with normal pupillary light reflexes and visual tracking, miosis OD, right facial hypalgesia, right head tilt, positional vertical nystagmus, and absent gag reflex. Proprioceptive placing decreased right thoracic limb, absent in the right pelvic limb	Right brainstem/cerebellar lesion
3	Twelve-year-old male English Springer Spaniel	One-week history of abnormal mentation, crying, pacing, and difficulty in walking	Obtunded with mild to moderate generalized ataxia and circling to the right. Proprioceptive placing decreased in pelvic limbs	Right cerebral or thalamic lesion
4	Twelve-year-old male castrated Labrador mix	Five-day history of generalized seizures and behavioral changes	Obtunded with mild tetraparesis and a right head turn. Proprioceptive placing decreased in all four limbs	Right cerebral or thalamic lesion
5	Seven-year-old male castrated Boxer	Eight-month history of generalized seizures; 1-month history of behavioral changes, mental dullness, and circling	Obtunded and pacing with circling to the right	Right cerebral or thalamic lesion

nificant mass effect and dilation of the right lateral ventricle. On transverse T1W images, the lesion was hypointense. There was no contrast enhancement until the final image, which showed minimal patchy enhancement (Fig. 5). Three weeks after the initial MRI study, a cystic lesion developed that had the same signal intensity as CSF on T1W images but was more hyperintense than CSF on T2W images.

All five tumors had marked peritumoral edema and a prominent mass effect (Table 2). The signal intensity on T1W images was iso- ($n = 3$) to hypointense ($n = 2$), and the T2W signal intensity was heterogenously hyperintense ($n = 5$). The post–contrast enhancement pattern was either uniform ($n = 1$), ring enhancing ($n = 3$), or minimal ($n = 1$) and also demonstrated that these tumors had a sharp ($n = 4$) or diffuse ($n = 1$) border. Apparent necrosis in all five tumors corresponded to intratumoral areas of low and high signal intensity on T1W and T2W images, respectively. A cystic lesion was diagnosed in two dogs, and these cysts were confirmed by pathologic examination.

CSF analysis

CSF from dog no. 1 had an elevated total protein (114 mg/dl) and a white blood cell (WBC) count of 12 cells/μl with a differential WBC of 1% neutrophils, 16% small mononuclear cells, 82% large mononuclear cells, and 1% eosinophils. No neoplastic cells were identified in the sample. In dog no. 2, the total protein was 15 mg/dl and the WBC count was 3 cells/μl. The differential WBC was 53% neutrophils, 6% small mononuclear cells, 36% large mononuclear cells, and 5% eosinophils. Again no neoplastic cells were identified. In dog no. 5, analysis of five consecutive CSF samples during a 3-month period revealed only an elevated total protein of 32 mg/dl in the second sample.

Gross pathology

Dog no. 1. No external macroscopic lesions were seen except that the pituitary stalk was slightly thickened and there was brownish discoloration of the median eminence. On transverse sections of the brain, a 2×2–cm well-demarcated, bilaterally symmetric area of brownish discoloration extended laterally on both sides of the hypothalamus from the optic chiasma to the mammillary bodies (Fig. 1a). The mass extended dorsally from the ventral surface of the hypothalamus to the fornix with displacement of the internal capsule and adjacent thalamus. The mass was sharply demarcated and had a soft gray rim of tumor tissue and a

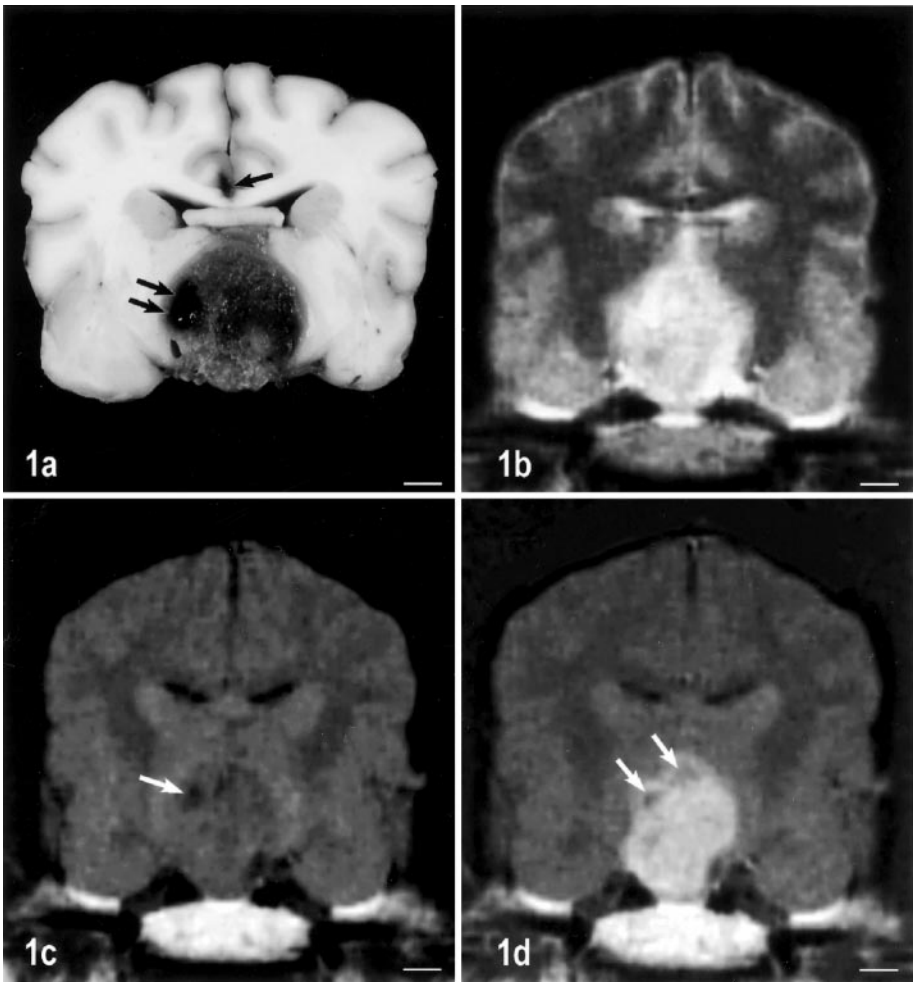

Fig. 1. Brain, GBM; dog no. 1. MRI and gross lesions of a transverse section at the level of the thalamus. **Fig. 1a.** Grossly, there was a 2 × 2–cm sharply demarcated round mass extending dorsally from the hypothalamus to the fornix with bilateral displacement of the thalamus and lateral ventricular compression. Overall, the mass had a granular texture, a soft gray rim of tumor tissue, focal areas of hemorrhage and necrosis, and a hemorrhagic cyst (double arrows). The focal hemorrhage in the left cingulate gyrus (arrow) was from the needle track of the CT-guided stereotactic biopsy. **Fig. 1b.** The transverse T2W image of the lesion shows a large area of hyperintensity. **Fig. 1c.** On the transverse T1W image, the lesion was iso- to hypointense. Note the hypointense area (arrow) corresponding to the cyst seen grossly. **Fig. 1d.** The T1W image demonstrates that the lesion had uniform contrast enhancement but was confined to a smaller area than abnormalities present on the T2W images. Two small nonenhancing hypointense areas (arrows) represent a cyst and focal necrosis. Bar = 0.5 cm.

granular texture with focal areas of recent hemorrhage, whitish yellow necrosis, and cyst formation (Fig. 1a). The pituitary gland was normal in size.

Dog no. 2. On external gross examination, there was a well-defined grayish mass with multiple yellowish and red foci that had extended to the ventrolateral margins of the right medulla oblongata. On transverse sections at this level, there was a 1.5-cm-diameter mass that had replaced most of the medulla on the right side.

Dog no. 3. No lesions were seen on external gross examination of the brain. On transverse sections, there was a large sharply demarcated mass in the right cerebral hemispheric white matter extending rostrocaudally 2.1 cm from the frontal lobe to the internal capsule. It extended mediolaterally about 1.8 cm from the midline of the corpus callosum within the corona radiata with the lateral margin bordered by the cortex of the parietal lobe. Dorsoventrally the tumor was up to 1.5 cm thick. The left ventricle was obliterated by the mass, and there was a pronounced mass effect with a left shift. Within the grayish tumor mass were random, multifocal areas of yellowish necrosis and acute hemorrhage.

Dog no. 4. On gross examination, there was a slight enlargement of the right frontal lobe and olfactory bulb, which transverse sections revealed was due to a well-demarcated gray to tan mass about 2.0 cm in di-

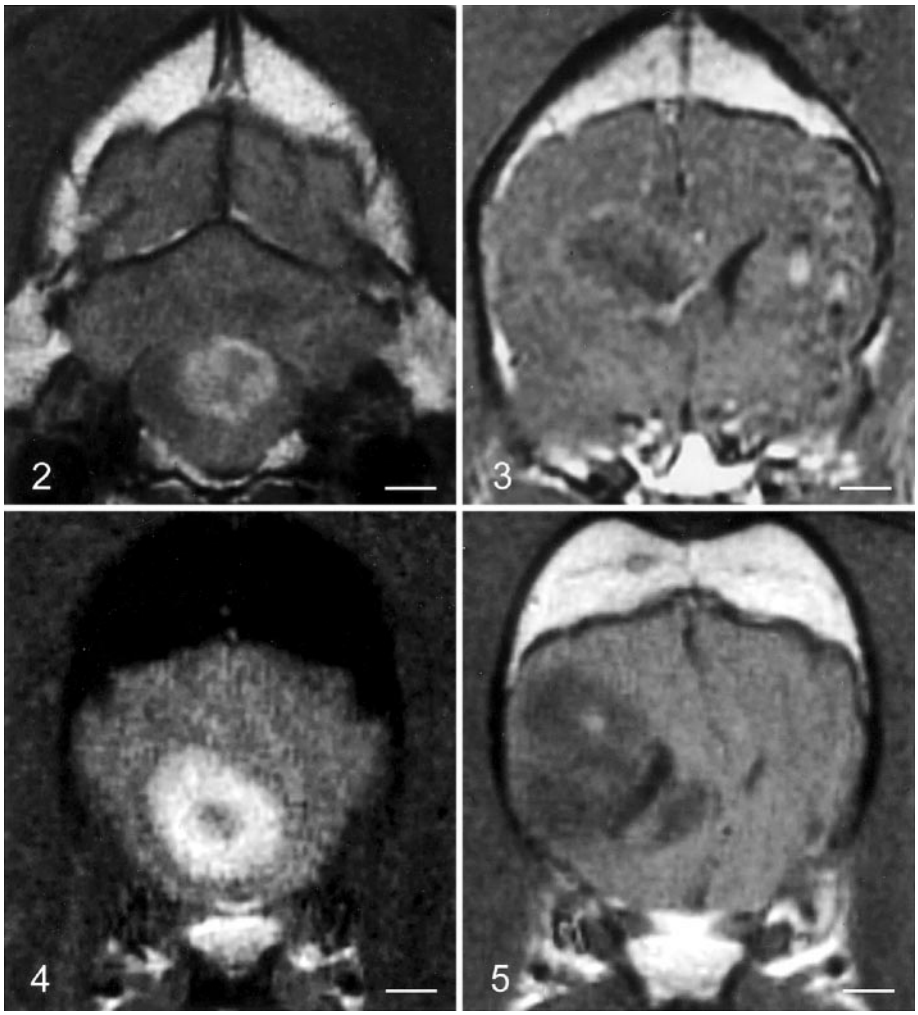

Fig. 2. Brain, GBM; dog no. 2. Transverse T1W post–contrast enhancement image with a thick ring of contrast enhancement in the right pons and medulla. Bar = 0.4 cm.

Fig. 3. Brain, GBM; dog no. 3. Transverse T1W post–contrast enhancement image. Note the thin rim of contrast enhancement around the hypointense tumor that compressed the right lateral ventricle. Bar = 0.4 cm.

Fig. 4. Brain, GBM; dog no. 4. Transverse T1W post–contrast enhancement image. There is a thick ring of enhancement involving the right olfactory bulb and the right frontal lobe. Bar = 0.4 cm.

Fig. 5. Brain, GBM; dog no. 5. Transverse T1W post–contrast enhancement image with minimal patchy enhancement. Note the prominent midline shift. Bar = 0.4 cm.

Table 2. MR imaging features of GBM in five dogs.*

Dog No.	Peritumoral Edema	Mass Effect	SI T1W	SI T2W	Contrast Enhancement	Apparent Necrosis	Border†	Cyst
1	+	+	Iso-hypo	Hetero	Uniform	+	Sharp	+
2	+	+	Iso-hypo	Hetero	Ring	+	Sharp	−
3	+	+	Iso-hypo	Hetero	Ring	+	Sharp	−
4	+	+	Hypo	Hetero	Ring	+	Sharp	−
5	+	+	Hypo	Hetero	Minimal	+	Diffuse	+

* SI = signal intensity; Hetero = heterogenous; Iso = isointense; Hypo = hypointense.
† Post–Gd-DTPA.

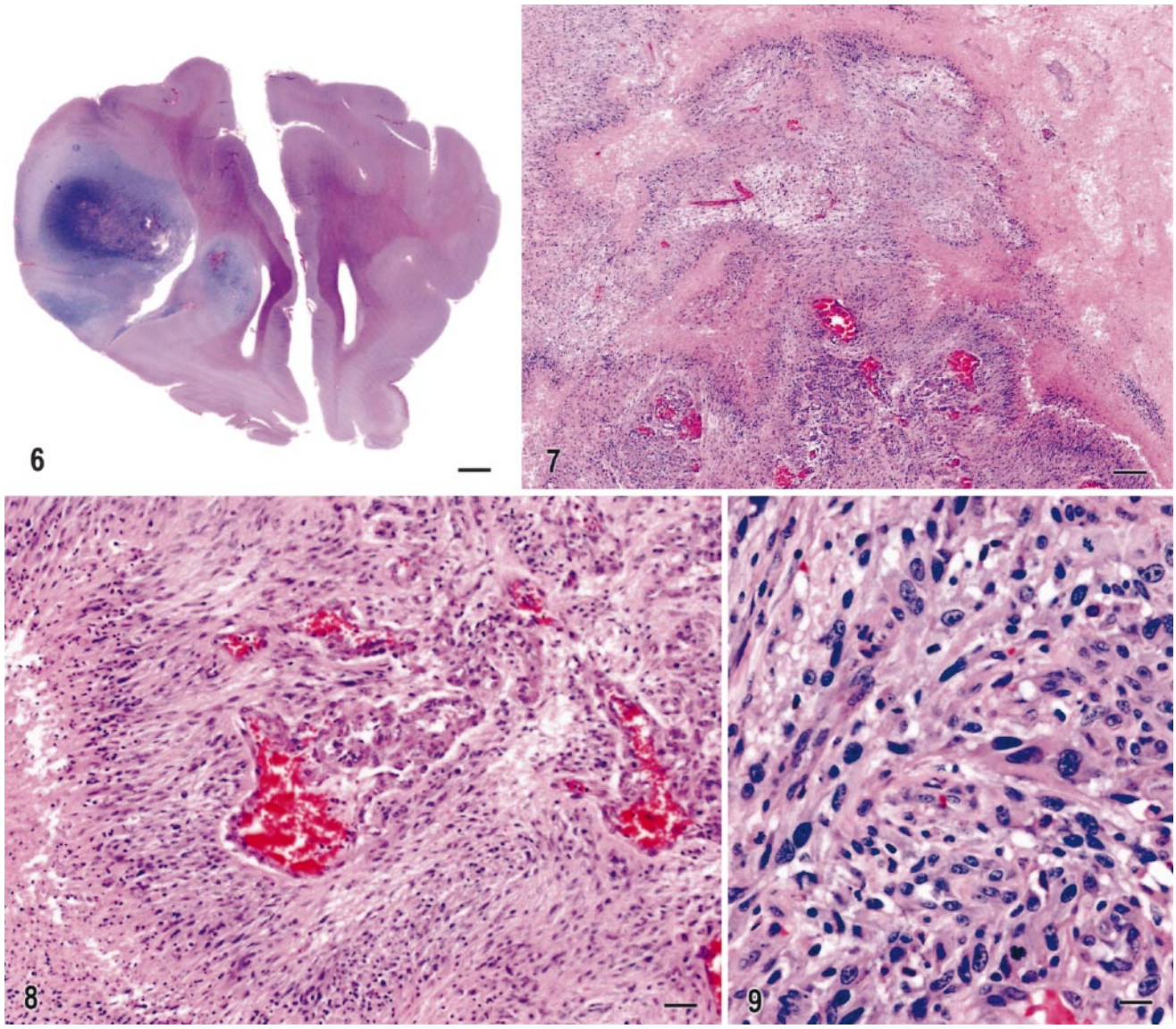

Fig. 6. Brain, GBM; dog no. 5. Macrophotograph of a transverse section illustrating the extent and distribution of tumor growth and a midline shift. There are multiple foci of intratumoral necrosis and hemorrhage. HE stain. Bar = 7 mm.

Fig. 7. Brain, GBM; dog no. 1. Section illustrating the patterns of extensive acute coagulation necrosis and also serpentine channels of necrosis; the latter is further delineated by pseudopalisading of glial cells. HE stain. Bar = 400 μm.

Fig. 8. Brain, GBM; dog no. 1. Note the serpentine pattern of necrosis, glial cell pseudopalisading, and multifocal microvascular proliferation. HE stain. Bar = 120 μm.

Fig. 9. Brain, GBM; dog no. 1. There is marked cellular pleomorphism and anisokaryosis, with normal and bizarre mitotic figures. HE stain. Bar = 40 μm.

ameter, which contained numerous foci of soft yellowish necrosis and acute hemorrhage. The mass extended medially to partially invade the right ventricle. Laterally, the margins blended into the gray matter. There was an accompanying left midline shift. The central canal of the spinal cord from cervical segments C1–C3 was dilated.

Dog no. 5. Externally, there was enlargement of the right cerebral hemisphere, which on transverse sections was due to a large grayish 1.5 × 3–cm mass extending caudally within the white matter from the rostral aspect of the right frontal lobe to the caudal extent of the internal capsule and caudate nucleus. The tumor extended laterally from the adjacent lateral ventricle to the outer cortical margins of the temporal and parietal lobes with loss of intervening normal architecture (Fig. 6). There was also partial compression of the right lateral ventricle. There were multiple areas of

yellowish white necrosis and focal hemorrhage throughout the tumor. The right hemisphere was greatly enlarged with a corresponding left shift.

Microscopic changes

Microscopic and immunocytochemical findings in the first case are reported in detail and in the other cases only differences from this tumor are described.

Dog no. 1. The mass was composed of a highly vascular and pleomorphic astrocytic tumor cell population interspersed with areas of serpentine necrosis bordered by pseudopalisading glial cells (Fig. 7). There were also larger areas of acute coagulative necrosis (Fig. 7) and prominent multifocal microvascular proliferations (Figs. 7, 8). Abnormally large, irregularly shaped, thin-walled blood vessels often with associated hemorrhage were prominent in some areas. Some vessel lumens in necrotic areas contained occlusive fibrin thrombi. Most tumor cells had typically ovoid to elongate nuclei with bipolar processes forming streaming patterns with a variable cell density. There was marked cellular pleomorphism and anisokaryosis (Fig. 9). There was a high mitotic index with both normal and bizarre mitotic figures. Pseudopalisading by smaller dark-staining fusiform glial cells occurred at the periphery of areas of serpentine necrosis (Figs. 7, 8). The microvascular proliferation included cords of vessels forming multiple tufts and was most prominent near areas of necrosis. At the periphery of the tumor there was neuronal satellitosis and perivascular and subpial tumor cell infiltrates. Cytologic findings from the smear preparation from a CT-guided stereotactic biopsy included increased cell density, pleomorphic tumor cells with refractile fibrillary processes, and mitotic figures, and there was occasionally focal microvascular proliferation (Fig. 10). Similar histologic lesions also including necrosis with pseudopalisading were observed in tissues prepared from the same stereotactic biopsy sample (Fig. 11).

Immunocytochemical staining of cytoplasmic processes for GFAP and vimentin was strongest in the more elongate and well-differentiated astrocytic tumor cells (Table 3, Fig. 12). However, there were marked differences in staining intensity of tumor cells throughout the tumor. Many cells forming the microvascular proliferations immunostained positively for both factor VIII–related antigen and CD31 or SMA (Fig. 13). In contrast, the large irregular thin-walled blood vessels had minimal positive immunoreactivity of their thin lining cells with either factor VIII or CD31 and were SMA negative. MIB-1 immunoreactivity demonstrated a proliferation index of up to 14% of all tumor cells (Fig. 14). Apoptotic cells were concentrated mainly in pseudopalisading cells bordering the branching zones of necrosis. There was no positive immunoreactivity in any tumors for low– and high–molecular weight cytokeratins. There was positive immunoreactivity for EGFR and VEGF of similar intensity and location to that demonstrated in the positive human GBM control tissue. Positive EGFR immunoreactivity of tumor cells, but not vasculature, was observed as granular, strong, and widespread cytoplasmic and membrane staining (Fig. 15). VEGF immunoreactivity with cytoplasmic localization was also restricted to focal clusters of tumor cells. Microvascular proliferations and dilated vessels were not immunoreactive to VEGF antibody. No preferential positive immunostaining of pseudopalisading glial cells with VEGF was seen in either the human GBM or the canine GBM tissue.

Dog no. 2. The main histologic difference from dog no. 1 was that this tumor was composed of a less-dense spindle cell population, which in a few areas had faint staining of an extracellular myxoid component sometimes collecting in small lakes. Pseudopalisading was very prominent at the border of the serpentine pattern of necrosis. Although highly vascular, there was less microvascular proliferation, fewer abnormally shaped vessels, and minimal acute hemorrhage in the tumor. The spindle cells were uniformly and strongly GFAP reactive. The proliferative index was up to 6%. There was positive EGFR and VEGF immunoreactivity in some areas of the tumor.

Dog no. 3. Overall, there were more areas of both acute coagulation necrosis and hemorrhage. Extension of tumor into the lateral ventricle was observed. There were a few small foci of oligodendroglial cells scattered throughout the predominant pleomorphic spindle cell component. Microvascular proliferation was less pronounced in the tumor but was florid in subependymal locations adjacent to the main tumor mass. MIB-1 immunostaining was observed in up to 19% of the tumor cell nuclei. Both VEGF and EGFR immunoreactivities were weakly positive.

Dog no. 4. There was extensive serpentine coagulative necrosis but less-prominent microvascular proliferation. There were a few areas of oligodendroglioma-like cell differentiation. The proliferative index from MIB-1 immunostaining was up to 16%.

Dog no. 5. Glial cell pseudopalisading at the edge of necrotic channels and focal microvascular proliferation were both very prominent. There were areas with clusters of small elongate cells admixed with a population of more loosely arranged and vacuolated cells. The proliferative index of 26% was the highest of all tumors.

Discussion

The results of our MRI and neuropathologic findings demonstrate that the MRI and pathologic features of spontaneous GBM in the five dogs are very similar

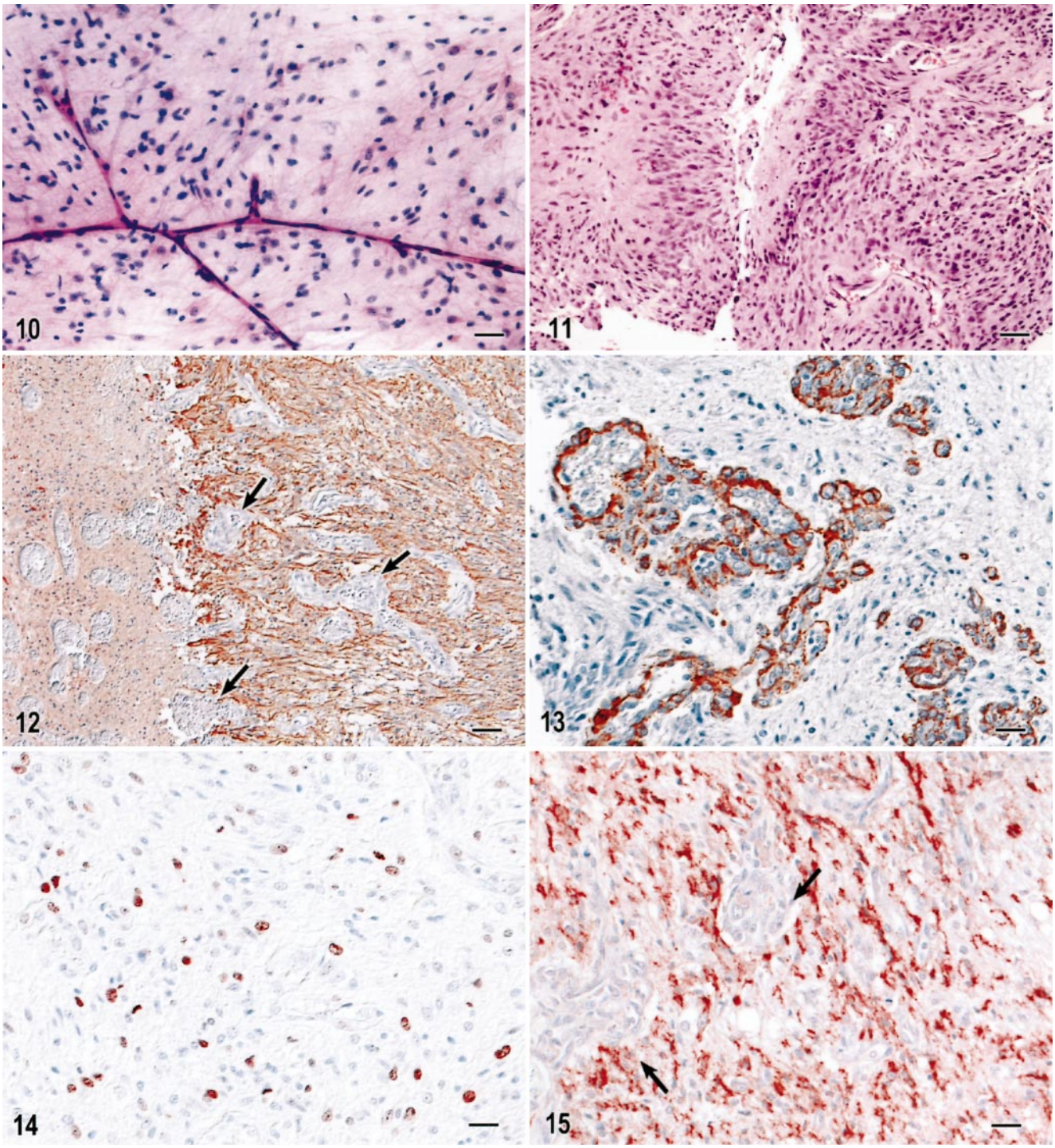

Fig. 10. Brain, GBM; dog no. 1. Smear from CT-guided biopsy tissue. There is increased cell density; tumor cells have elongate- to irregular-shaped nuclei with prominent cytoplasmic fibrillar processes. Note the branching capillaries. Rapid HE stain. Bar = 46 μm.

Fig. 11. CT-guided stereotactic biopsy sample. There is increased cellularity of the elongate to angular tumor cells with areas of necrosis and pseudopalisading. HE stain. Bar = 80 μm.

Fig. 12. Brain, GBM; dog no. 1. GFAP-positive immunoreactivity of tumor cells is observed but not the islands of neovascularization (arrows). To the left of the vertical border of demarcation is the necrotic tissue. GFAP stain. Streptavidin–biotin–peroxidase. Bar = 90 μm.

Fig. 13. Brain, GBM; dog no. 1. Note the positive immunoreactivity for SMA in pericytes within the microvascular proliferations. Streptavidin–biotin–peroxidase. Bar = 60 μm.

Table 3. Results of immuno- and histochemical reactivity of each of the canine GBM cases.

	Dog No. 1	Dog No. 2	Dog No. 3	Dog No. 4	Dog No. 5
GFAP	+	+	+	+	+
Cytokeratin	−	−	−	−	−
Factor VIII	+	+	+	+	+
CD31	+	+	+	+	+
SMA	+	+	+	+	+
VEGF	+	+	−	−	−
EGFR	+	+	+	−	−
MIB-1%	14	6	19	16	26
Apoptosis	+	+	+	+	+

to those characteristic of human GBM.[2,4,12,13,21] Because in human brain tumors combined interpretation of neuroimaging and pathology features is useful to optimize both diagnostic and prognostic information, we have chosen this approach also in reporting these canine GBMs.[4,12]

Many of the MRI features generally observed with human GBM occurred in the five dogs in this series. Most human GBMs exhibit a minimal to slightly hypointense signal on T1W images with a pronounced mass effect.[2,21,22,25] On the T1W canine images, three dogs had minimal signal change, whereas the other two tumors were hypointense. All the tumors were associated with a marked mass effect. In human GBM, T2W images demonstrate a heterogenous mixture of hypo- and hyperintense areas within the tumor.[2,21] The T2W images in these dogs were hyperintense with some heterogeneity. Peritumoral edema is a consistent finding in human GBM and was also demonstrated in all five canine tumors.[2,21,25] In human GBM, contrast agents can demonstrate focal, mixed, or ring patterns of enhancement.[2,21,25] The enhancement is believed to be mainly from increased vascular permeability due to tumor angiogenesis and exacerbated by a loss of blood-brain barrier integrity.[25] Post–Gd-DTPA imaging studies demonstrated that three dogs had ring-enhancing lesions, one had uniform enhancement, and one had minimal enhancement. The areas of low and high signal intensity on T1W and T2W images, respectively, which also did not enhance with Gd-DPTA, were correlated with areas of necrosis on pathologic examination.[22] Necrosis associated with ring enhancement was found in all five tumors. These presumed cystic lesions corresponded topographically to those found at gross necropsy examination. Although the number of dogs in this study is too small for definitive statistical analysis of these MRI findings, there is nevertheless a high level of concordance of MRI features with those of human GBM. The diagnostic relevance of these MRI findings in the dog, however, must await comparable studies on other types of histologically classified and graded astrocytomas and also between other glial tumors.

Two previous studies of canine astrocytomas, comprising 11 dogs, did not report any overall consistency of their MRI findings.[16,29] However, a useful correlation is demonstrated between the MRI features and each of the histologic grades of human astrocytomas.[2,4,12,21] Also, it is recognized that canine astrocytomas have the same histologic subtypes as their human counterparts, although their frequency and overall rate of occurrence differ quite dramatically from humans.[15,28] If the WHO grading system had been applied in the canine astrocytoma studies, a similar correlation between the MRI features and the histologic type may have been detected.

There were both gross and microscopic lesions in this series of canine tumors, consistent with those described in human GBM.[4,12,13,27] First, four of the tumors occurred supratentorially. Second, consistent gross lesions were focal areas of necrosis and hemorrhage, which were seen as variegated areas in four of the tumors. In two tumors, cyst formation as suggested by MRI was confirmed pathologically. Third, mass effects and peritumoral edema causing midline shifts occurred in all tumors.[4,12]

Human GBMs share with WHO grade III astrocytomas histologic features of increased cellularity, pleomorphism, nuclear atypia, and mitotic activity. However, essential for the exclusive diagnosis of human GBM are the added features of prominent microvascular proliferation and necrosis with pseudopalisading, which therefore distinguish them from grade III astrocytomas.[4,12,13] Histologically, the canine tumors were each composed of a heterogenous spindle cell population with marked anaplasia, anisokaryosis, and prominent mitotic activity. One or both of the cardinal features of necrosis or microvascular proliferation, essential for the histologic diagnosis of human GBM, were present in all the canine tumors.[4,12,13] The only

←

Fig. 14. Brain, GBM; dog no. 1. MIB-1 immunoreactivity with a proliferative index of about 14%. Streptavidin–biotin–peroxidase. Bar = 50 μm.

Fig. 15. Brain, GBM; dog no. 2. Positive immunoreactivity to EGFR within a focal area of the tumor. Islands of microvascular proliferation are minimally immunoreactive (arrows). Bar = 45 μm.

histologic differences between the canine tumors were in the density of pseudopalisading glial cells bordering the necrosis, the extent of the microvascular proliferation, the degree of increased cellularity, and the intensity of GFAP immunoreactivity of the tumor cells. Positive immunoreactivity for GFAP varied between different populations of astrocytoma cells with the weakest staining in small, dark round cells and larger cells. Tumor cells with elongate nuclei and cytoplasmic processes stained most intensely. Large multinucleated cells are sometimes seen in very pleomorphic human tumors. Their presence is not obligatory for the diagnosis, has no prognostic significance, and was not observed in any of the canine tumors.[4,12] The microvascular proliferation consisted of endothelial cell hyperplasia in small vessels associated with tumor angiogenesis.[3,4,12,24] These microvascular proliferations occurred usually near the periphery of necrotic areas or in long curving aggregates within or near the edge of the tumor. Many of these vessels also had a substantial smooth muscle cell component as demonstrated by their SMA immunoreactivity. In human GBM, endothelial and smooth muscle cell proliferation is attributed to paracrine secretion of VEGF and PDGF, respectively, by tumor cells.[8,9,24] In the canine tumors, as in human GBMs, the thin-walled telangiectatic blood vessels exhibited minimal staining of their lining cells and no smooth muscle cell hyperplasia. All the tumors also exhibited intratumoral necrosis in two main patterns.[4,12] One pattern occurred as extensive broad well-defined areas of acute coagulative necrosis of both parenchyma and blood vessels. The second pattern was of branching serpentine channels of necrosis usually bordered by palisading glial cells oriented perpendicularly to this necrotic tissue. The stellate or fascicular cell patterns in some areas sometimes had a diffuse or lakelike interstitial accumulation of myxoid material. Small foci of oligodendroglial cell morphology were found in two tumors. These diverse histologic findings in part reflect the heterogeneity of the cellular type and patterns that underscore the multiforme designation of the tumor and are considered inclusive within the spectrum of the human GBM.[4,12,13]

Some of the histologic features considered indicative of a migratory and invasive capability of tumor cells, including subpial and perivascular neoplastic cell infiltrates and neuronal satellitosis, occurred around the periphery of three tumors.[28] Proliferative indices in human GBMs have been reported to be between 5% and 30% with an average value around 25% using MIB-1 antibody, but it still remains to be shown whether this index has reliable prognostic value.[4,12,13] The range in our canine cases between 6% and 26% appears comparable, but further prospective studies of the prognostic relevance of such indices are obviously needed.

Deregulation of some genes involved in the control of cell growth and angiogenesis has been demonstrated in many human GBMs and particularly in those of EGFR and VEGF.[12,31] EGFR gene amplification occurs at a high frequency in more than 40% of human GBMs with increased gene expression, as detected immunocytochemically in $>$ 60% human tumors. To date, however, these alterations have not had any predictive significance.[12,20] Comparably in this canine series, 60% ($n = 3$) of the GBMs had increased expression of EGFR as detected by positive immunoreactivity. Experimental evidence suggests that VEGF isoforms alone are primarily responsible for initiation of angiogenesis in murine models.[3,9] High levels of VEGF expression have been shown immunocytochemically in human GBMs, particularly in pseudopalisading glial cells.[5,11,19] Upregulated expression of VEGF was detected immunocytochemically in 40% of these canine tumors in patterns similar to those described in human GBMs.[5,11,12,23] However, immunoreactivity of pseudopalisading cells was not the feature sometimes reported in human tumors, but this difference might be attributed to the antibody source and specificity. Although no molecular genetic studies have been reported to date with canine brain tumors, our findings suggest the occurrence of underlying mutational events possibly similar to those in human GBMs.[12,20,31]

Acknowledgements

We thank Drs. B. K. Sturges, K. M. Vernau, H. Rylander, D. W. Agnew, D. MacAloose, J. A. Werner, and M. K. Keel for their excellent help with the clinical examination or necropsy of these cases and Mr. S. Maslowski for his superb help with the neuroimaging studies of these dogs.

References

1 Anor S, Sturges BK, LaFranco L, Jang SS, Higgins RJ, Koblik PD, LeCouteur RA: Systemic phaeohyphomycosis (*Cladophialophora bantiana*) in a dog—clinical diagnosis with stereotactic CT-guided brain biopsy. J Vet Intern Med **15:**257–261, 2001

2 Atlas SW, Lavi E: Intra-axial brain tumors. *In*: Magnetic Resonance Imaging of the Brain and Spine, ed. Atlas SW, 2nd ed., pp. 315–422. Lippincott-Raven, Philadelphia, PA, 1996

3 Brat DJ, Van Meir EG: Glomeruloid microvascular proliferation orchestrated by VPF/VEGF. Am J Pathol **158:** 789–796, 2001

4 Burger PC, Scheithauer BW: Tumors of the neuroglia and choroid plexus epithelium. *In*: Tumors of the Central Nervous System. Atlas of Tumor Pathology, pp. 25–148. AFIP, Washington, DC, 1993

5 Chein MR, Plate KH: VEGF in brain tumors. J Neurooncol **50:**109–120, 2000

6 Dickinson PJ, Keel MK, Higgins RJ, Koblik PD, Le-

Couteur RA, Naydan DK, Bollen AW, Vernau W: Clinical and pathologic features of oligodendrogliomas in two cats. Vet Pathol **37:**160–167, 2000
7 Dunn IF, Heese O, McBlack P: Growth factors in glioma angiogenesis: FGFs, PDGF, EGF, and TGFs. J Neurooncol **50:**121–137, 2000
8 Haddad SF, Moore SA, Schelper RL, Goeken JA: Vascular smooth muscle hyperplasia underlies the formation of glomeruloid vascular structures of glioblastoma multiforme. J Neuropathol Exp Neurol **51:**488–492, 1992
9 Hanahan D, Folkman J: Patterns and emerging mechanisms of the angiogenic switch during tumorigenesis. Cell **86:**353–364, 1996
10 Higgins RJ, LeCouteur RA, Vernau KM, Sturges BK, Obradovich JE, Bollen AW: Granular cell tumor of the canine central nervous system: two cases. Vet Pathol **38:** 620–627, 2001
11 Johansson M, Brannstrom T, Bergenheim T, Henrikson R: Spatial expression of VEGF-A in human glioma. J Neurooncol **59:**1–6, 2002
12 Kliehues P, Burger PC, Collins VP, Newcombe EW, Ohgaki H, Cavenee WK: Glioblastoma. *In*: Pathology and Genetics of Tumours of the Nervous System, ed. Kliehues P, Cavenee WK, pp. 29–39. IARC Press, Lyon, France, 2000
13 Kliehues P, Louis DN, Scheithauer BW, Rorke LB, Reifenberger G, Burger PC, Cavenee WK: The WHO classification of tumors of the nervous system. J Neuropathol Exp Neurol **61:**215–225, 2002
14 Koblik PD, LeCouteur RA, Higgins RJ, Bollen AW, Vernau KM, Kortz GD, Ilkiw JE: CT-guided brain biopsy using a modified Pelorus Mark III stereotactic system: experience with 50 dogs. Vet Radiol Ultrasound **40:**434–440, 1999
15 Koestner A, Higgins RJ: Tumors of the nervous system. *In*: Tumors of Domestic Animals, ed. Meuten DJ, pp. 697–738. Iowa State University Press, Ames, IA, 2002
16 Kraft SL, Gavin PR, DeHaan C, Moore M, Wendling LR, Leathers CW: Retrospective review of 50 canine intracranial tumors evaluated by magnetic resonance imaging. J Vet Intern Med **11:**218–225, 1997
17 Lenz SD, Janovitz EB, Lockridge K: An anaplastic astrocytoma (glioblastoma) in the cerebellum of a dog. Vet Pathol **28:**250–252, 1991
18 Luginbuhl H, Fankhauser R, McGrath JT: Spontaneous neoplasms of the nervous system in animals. *In*: Progress in Neurological Surgery, ed. Krayenbuhl H, Maspes PE, and Sweet WH, vol. 2, pp. 103–104. Karger, Basel and Year Book, Chicago, IL, 1968
19 Macheim MR, Plate KH: VEGF in brain tumors. J Neurooncol **50:**109–120, 2000
20 Newcombe EW, Cohen H, Lee SR, Bhalla SK, Bloom J, Hayes RL, Miller DC: Survival of patients with glioblastoma multiforme is not influenced by altered expression of p16, p53, EGFR, MDM2 or Bcl-2 genes. Brain Pathol **8:**655–667, 1998
21 Orrison WW, Hart BL: Intra-axial brain tumors. *In*: Neuroimaging, ed. Orrison WW, pp. 583–598. WB Saunders, Philadelphia, PA, 2000
22 Pierallini A, Bonamini M, Ponano P, Pameggiani, Raguso M, Osti MF, Anaveri G, Bozzao L: Radiological assessment of necrosis in glioblastoma: variability and prognostic value. Neuroradiology **40:**150–153, 1998
23 Pietsch T, Valter MM, Wolf HK, von Deimling A, Huang H-JS, Cavanee WK, Wiestler OD: Expression and distribution of vascular endothelial growth factor protein in human brain tumors. Acta Neuropathol **93:**109–117, 1997
24 Plate KH, Breier G, Weich HA, Risau W: Vascular endothelial growth factor is a potential tumor angiogenesis factor in human gliomas in vivo. Nature **359:**845–848, 1992
25 Pronin IN, Holodny AI, Petraikin AV. MRI of high-grade glial tumors: correlation between the degree of contrast enhancement and the volume of surrounding edema. Neuroradiology **39:**348–350, 1997
26 Scheifer B, Dahme E: Primare Geschwulste des ZNS bei Tieren. Acta Neuropathol **2:**202–212, 1962
27 Scherer HJ: The forms of growth in gliomas and their practical significance. Brain **63:**1–35, 1940
28 Summers BA, de Lahunta A, Cummings JF: Tumors of the nervous system. *In*: Veterinary Neuropathology, ed. Summers BA, de LaHunta A, Cummings JF, pp. 363–368. Mosby-Year Book, Inc., St Louis, MA, 1995
29 Thomas WB, Wheeler SJ, Kramer R, Kornegay JN: Magnetic resonance imaging features of primary brain tumors in dogs. Vet Radiol Ultrasound **37:**20–27, 1995
30 Vernau KM, Higgins RJ, Bollen AW, Jimenez DF, Anderson JV, Koblik PD, LeCouteur RA: Primary canine and feline nervous system tumors: intraoperative diagnosis using the smear technique. Vet Pathol **38:**47–57, 2001
31 Watanabe K, Tachibana O, Sato K, Yonekawa Y, Kliehues P, Ohgaki H: Overexpression of the EGFR receptor and p53 mutations are mutually exclusive in the evolution of primary and secondary glioblastomas. Brain Pathol **6:**217–224, 1996

Request reprints from Dr. R. J. Higgins, Department of Pathology, Microbiology, and Immunology, Haring Hall, School of Veterinary Medicine, University of California–Davis, Davis, CA 95616 (USA). E-mail: rjhiggins@ucdavis.edu.